Central European Journal of Energetic Materials, **2014**, *11*(2), 257-269
ISSN 1733-7178

An Investigation of the Preparation and Performance of Microcellular Combustible Material

Weitao YANG, Yuxiang LI and Sanjiu YING*

School of Chemical Engineering, Nanjing University of Science and Technology, Nanjing 210094, China
**E-mail: yingsanjiu@126.com*

Abstract: Microcellular combustible materials, based on poly(methyl methacrylate) (PMMA) bonded RDX, were fabricated by the pressure quench method using supercritical CO_2. After foaming, the bulk density, porosity, expansion ratio and cell density were analyzed. Scanning Electron Microscopy (SEM) has also been used to investigate the influence of the foaming conditions (temperature, saturation pressure and depressurization time) and the RDX ratio on the porous structure. The skin-core structure was also observed after the pressure quench process. The mechanical sensitivities and burning performance were investigated by the friction sensitivity test, the impact sensitivity test and the closed vessel test, respectively.

Keywords: microcellular combustible material, supercritical CO_2, pressure quench method, vulnerability behaviour, closed vessel test

1 Introduction

Microcellular combustible materials based on polymer bonded RDX possess several advantages such as an adjustable energy content, high burn rate and low vulnerability [1]. The materials can burn out in a reduced time for a giant internal surface area, leaving no burn residue. These materials have immense potential for application in combustible cartridge cases [2-5] and caseless ammunition [6-8]. Furthermore, future applications such as compact or modular charges, the fixing of ammunition components by foam and gradient charges can also be achieved. In recent years, a reaction injection moulding (RIM) process has been designed to produce foamed polymer bonded RDX propellants with low

vulnerability [6, 7]. Good performance in burning and sensitivity behaviour may allow their use as superior replacements of conventional porous materials in several of the applications mentioned above.

In our previous work, microcellular nitrocellulose-based propellants have been fabricated successfully by a two-step foaming process using supercritical CO_2 as the foaming agent [9-11]. Supercritical CO_2 exists as a non-condensable, high density fluid above its critical temperature (31.1 °C) and critical pressure (7.38 MPa). In addition, CO_2 in the supercritical state is an inexpensive, safe and environmentally benign blowing agent [12]. In the fabrication of foams, the most accessible control methods for the foaming process are changes in saturation pressure, foaming temperature, depressurization rate and the restriction level of the foaming moulds [13-16]. In this paper, combustible microcellular materials were foamed without the restraint of foaming molds in order to obtain a lower bulk density. The influence of the foaming conditions and the RDX content on the internal porous structure are discussed. The performance, including vulnerability and combustion, were also investigated.

2 Experimental Section

2.1 Materials and preparation of microcellular combustible material

The basic formulation was composed of RDX and an inert binder. The average particle size of the fine RDX was 10 μm and the inert binder was poly(methyl methacrylate) (PMMA) (Altuglas® V 040). RDX and the binder were blended, kneaded, and extrusion moulded to form the desired shape and then dried by traditional methods.

The above solid specimens were cut to 50 mm × 12.9 mm× 2 mm and foamed by the pressure quench foaming process (one-step foaming process) in a device shown in Figure 1. The major steps are as follows: (a) preheat the high pressure vessel in a water-bath to a certain temperature, above the critical temperature; (b) place the solid specimen in the vessel; (c) having flushed the vessel for a few minutes with CO_2, pump CO_2 into the vessel and raise the internal pressure to the desired pressure, above the critical pressure, then close the valve; (d) expose the solid specimen in SC-CO_2 for 10 h; (e) open the vessel after releasing the pressure during a predetermined time and remove the specimen.

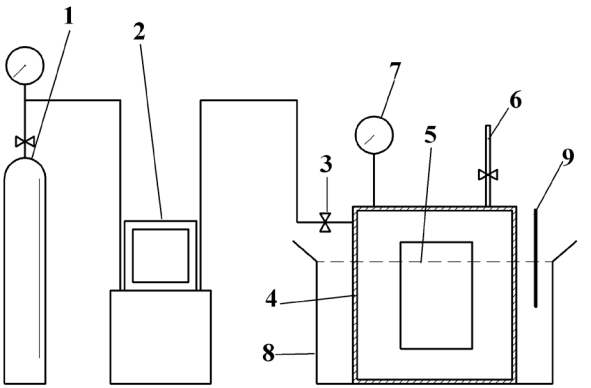

Figure 1. Schematic illustration of the foaming process in SC-CO_2. 1 − CO_2 gas cylinder; 2 − Plunger type metering pump; 3 − Gas inlet value; 4 − High pressure vessel; 5 − Specimen; 6 − Gas-release valve; 7 − Piezometer; 8 − Thermostatic water bath; 9 − Thermometer.

2.2 Inner structure characterization

The density of the microcellular specimens was measured using Xu's method [14] as Equation (1):

$$\rho = \omega_1 \rho_w / (\omega_1 + \omega_2 - \omega_3) \tag{1}$$

where ρ (g/cm^3) is the density of the specimen; ρ_w (g/cm^3) is the density of water, ω_1 (g) is the weight of the specimen; ω_2 (g) is the weight of the bottle filled with water; and ω_3 (g) is the weight of the bottle containing both water and the specimen.

The expansion ratio (φ) is the ratio of the density of the solid specimen (ρ_s) and the density of the microcellular specimen (ρ_f).

$$\varphi = \rho_s / \rho_f \tag{2}$$

The void fraction V (%) was calculated by Equation (3).

$$V = 1 - 1/\varphi \tag{3}$$

The foamed propellant grains were sputtered with gold for 6 min under vacuum conditions in a gold-spraying apparatus (EMITECH K550X Sputter Coater); the electric current was 30 mA. The morphology was observed and recorded by SEM

using QUANTA FEG 250 type in a 5 kV accelerating electric field. The porous structure was observed from the SEM micrographs. The cell density (the number of cells per cubic centimeter of specimen) was calculated from Equation (4):

$$N_0 = \left(\frac{n\mathrm{M}^2}{\mathrm{A}}\right)^{\frac{3}{2}} \times \varphi \quad (\mathrm{cells/cm^3}) \tag{4}$$

where n is the number of cells on the SEM micrograph, M is the magnification factor, and A is the area of the micrograph (cm^2).

2.2 Tests of mechanical sensitivities

The schematic diagram of the friction sensitivity test apparatus is shown in Figure 2. The primary parts of the test apparatus are the moving anvils between which the test sample is placed, a plunger that applies a load to the sample, and a swinging pendulum that strikes the ram to move the upper moving anvil. The pendulum is positioned and released at such an angle that it will impart a predetermined velocity to the sliding anvil. The travel distance of the sliding anvil is approximately 2 mm. Explosion of the sample was determined by the production of smoke, fire or an audible pop. The experimental conditions were chosen according to Table 1. Three samples with mass 30 ± 1 mg were tested at 96 ± 1° and 4.90 ± 0.007 MPa. Fifty tests were carried out to obtain the mean explosion probability ($\overline{P}$, %).

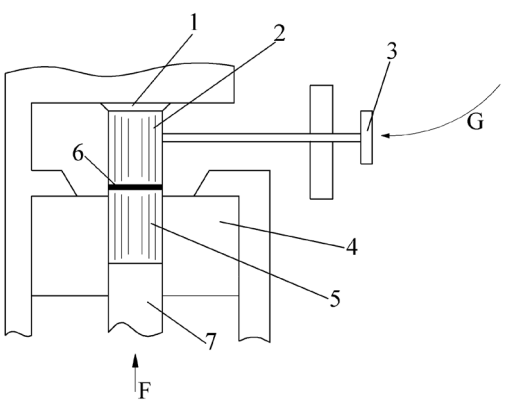

Figure 2. Schematic diagram of the friction sensitivity test apparatus. 1 − Top plate; 2 − Upper sliding anvil; 3 − Ram; 4 − Guide sleeve; 5 − Lower moving anvil; 6 − Sample; 7 − Plunger; F − Applied force direction; G − Pendulum striking direction.

Table 1. Experimental conditions for the friction sensitivity test

Angle [°]	Pressure [MPa]	Mass of sample [mg]	Test sample
66 ±1	2.45 ±0.07	20 ±1	General powder
96 ±1	4.90 ±0.07	30 ±1	Powder with low sensitivity
90 ±1	3.92 ±0.07	20 ±1	Powder with moderate sensitivity
80 ±1	2.45 ±0.07	20 ±1	Powder with high sensitivity

An up-and-down method was used for the statistical calculation. The actual starting place for recording data was found by a series of ranging shots. By having the first drop to occur well above an assured explosion height, the height bar was lowered in two step size intervals until a non-explosion occurred. After the first non-explosion occurred, the bar was raised one test interval and the recording of data was commenced. By using the ranging method for determining the starting point, a greater percentage of the data collected fell near the mean. A complete test consisted of a series of 25 effective shots. The impact sensitivity obeys a logarithmic normal distribution and consequently $\overline{H}_{50}$ can be statistically calculated. The impact sensitivities of 3 samples with mass 50 ± 1 mg were characterized by their characteristic drop height ($\overline{H}_{50}$), which was calculated from 25 effective test values obtained using a 5 kg drop-hammer.

2.3 Closed vessel test

The burning characteristics of the specimens were investigated using a 109 mL constant volume, closed vessel. The initial atmosphere in the vessel was air. All of the samples were tested with a loading density of 0.20 g/cm^3. Specimens were fired using nitrocellulose with a nitrogen content of 12.0%. The igniting pressure was 10.98 MPa and the data sampling interval was 0.001 ms.

3 Results and Discussion

3.1 Dispersion of RDX particles in polymer matrix

The dispersion of RDX particles in the binder matrix using the solvent method was tested first and the result is shown in Figure 3. As the figure indicates, RDX particles are embed in the matrix and are dispersed uniformly without agglomeration.

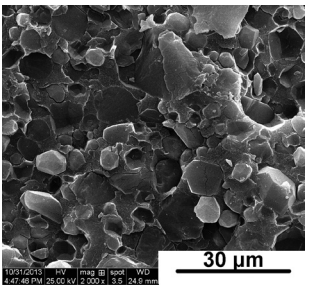

Figure 3. SEM micrograph of an un-foamed specimen (RDX ratio = 60%).

3.2 Porous morphology characterization

In the foaming procedure, heterogeneous nucleation was generated around the RDX particles, and homogeneous nucleation was generated in the polymer matrix. After pressure quenching, the cells are not generated simultaneously, because the energy-barrier for heterogeneous nucleation around the RDX particles is three orders of magnitude lower than that of homogeneous nucleation in the polymer matrix [17]. Therefore, preferential nucleation of cells around the RDX particles consumes a large amount of gas, which decreases the gas concentration in the adjacent matrix. Homogeneous nucleation in the matrix can be generated before the gas concentration has decreased below the critical concentration for nucleation, unless it has a high nucleation rate which is influenced by temperature, gas concentration and depressurization rate [18-20].

3.2.1 Effect of foaming temperature on the porous morphology

Figure 4 shows the effect of the foaming temperature on the porous morphology. As shown in Figure 4, a drastic change in morphology is observed with increased temperature. At 40 and 50 °C, only heterogeneous nucleation around the RDX particles occurred and closed-cell structures were observed. But at 60 and 70 °C, higher magnification revealed a clear bimodal cell structure, consisting of homogeneous and heterogeneous pores. Figure 4 also indicated an increase in pore size with increasing temperature. Table 2 presents the structural parameters of the microcellular specimens foamed at different temperatures; these data indicate that the porosity and expansion ratio generally increase with foaming temperature.

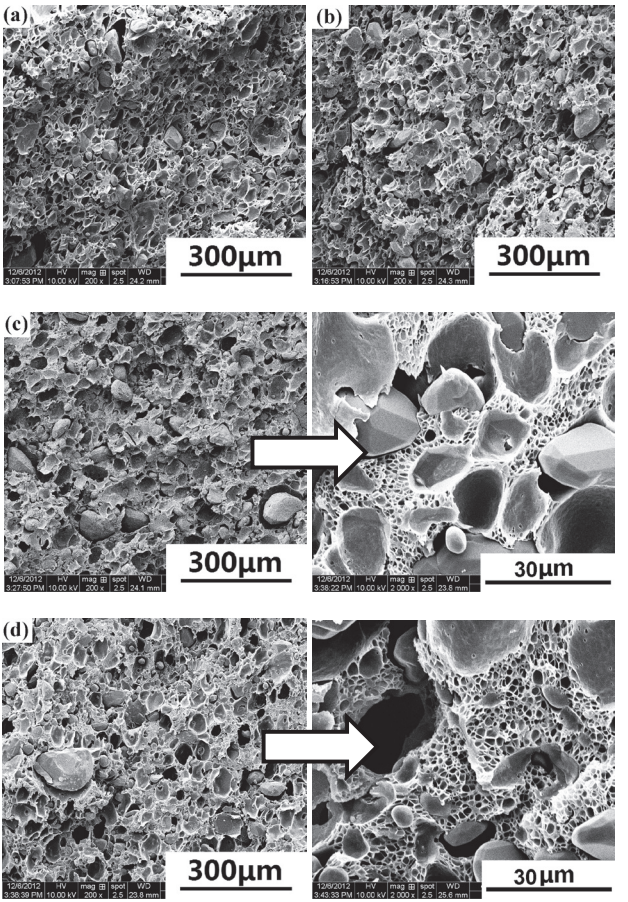

Figure 4. SEM micrographs of specimens foamed at different temperatures (pressure = 20 MPa, RDX ratio = 60%, time = 10 s): (a) 40 °C; (b) 50 °C; (c) 60 °C; (d) 70 °C.

Table 2. Values of ρ_f, φ and V of the microcellular specimens foamed at different temperatures

Foaming temperature [°C]	40	50	60	70
ρ_f [g/cm^3]	0.89	0.83	0.86	0.73
φ	1.69	1.81	1.74	2.05
V [%]	40.8	44.8	42.5	51.2

3.2.2 Effect of saturation pressure on the porous morphology

Sorption levels are increased with increased pressure when the temperature is

constant. Additionally, the homogeneous nucleation rate increases with increased pressure drop during a 10 s depressurization time. Thus, cells generated by homogeneous nucleation emerge in the matrix, which is indeed observed in Figure 5. A bi-modal cell structure was formed at a higher pressure of 25 MPa at 50 °C and the microcells were much smaller than those shown in Figure 4. Table 3 presents the structural parameters of the microcellular specimens foamed at different pressures; these data reveal specimens with a bi-modal structure and larger porosity.

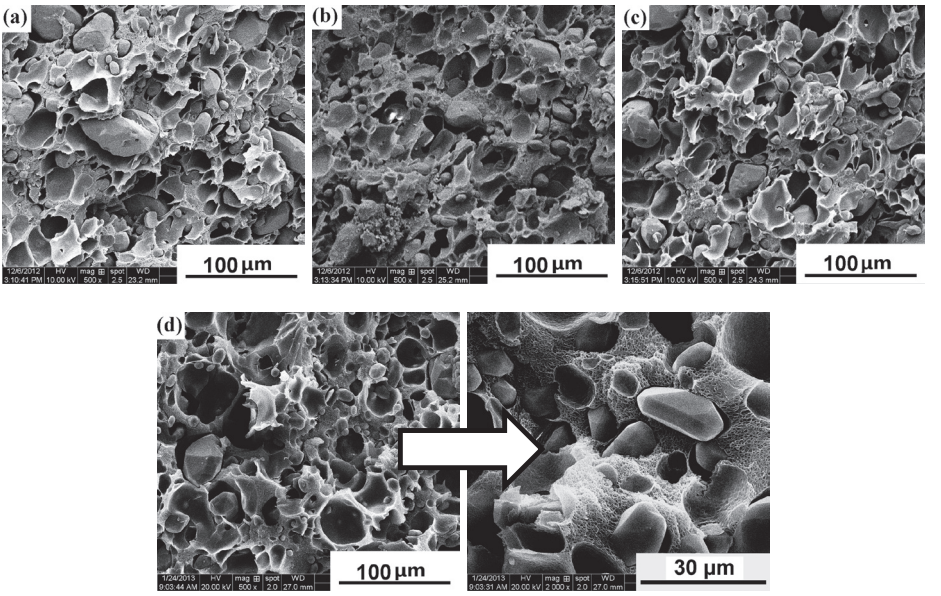

Figure 5. SEM micrographs of specimens generated at different pressures (temperature = 50 °C, RDX ratio = 60%, time = 10 s): (a) 10 MPa; (b) 15 MPa; (c) 20 MPa; (d) 25 MPa.

Table 3. Values of ρ_f, φ and V of the microcellular specimens foamed at different pressures

Pressure [MPa]	10	15	20	25
ρ_f [g/cm^3]	0.87	0.82	0.83	0.76
φ	1.72	1.83	1.81	1.97
V [%]	41.8	45.4	44.8	49.2

3.2.3 Effect of depressurization time on the porous morphology

Another adjustable parameter influencing the foam morphology is the depressurization rate. The influence of the depressurization rate on the foam

morphology was studied for specimens equilibrated at a constant pressure and temperature, 15 MPa and 50 °C respectively. In Figure 6, three micrographs of specimens foamed during different depressurization times are presented. As the depressurization time is increased, the cells are formed over a longer growth period, resulting in a larger pore size and inhomogeneous size distribution.

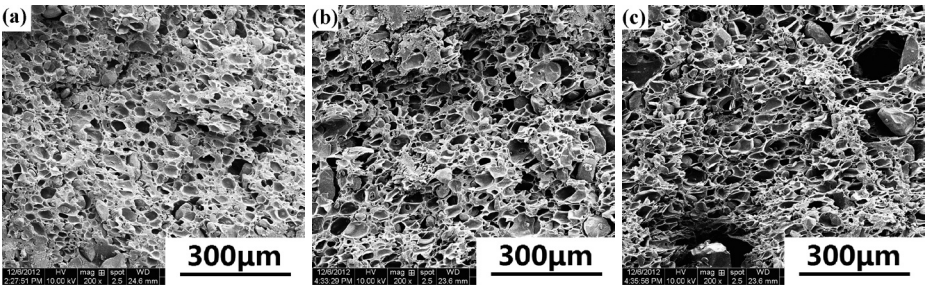

Figure 6. SEM micrographs of specimens foamed over different depressurization times (temperature = 50 °C, pressure = 15 MPa): (a) 10 s; (b) 90 s; (c) 8 min.

3.2.4 Effect of RDX content on heterogeneous nucleation

RDX particles act as oxidants as well as nucleating agents. In order to study the effect of RDX particles on the heterogeneity, specimens with different RDX ratios were foamed at 50 °C after being saturated at 20 MPa. A statistical calculation on the cell size and the sum of the cells was performed using the SEM images. Figure 7 shows SEM micrographs of microcellular specimens as a function of RDX ratio, and Table 4 presents the structural parameters of these foamed specimens. As shown in Table 4, the cell density increased with increasing RDX ratio, resulting from the increased nucleation sites. Specimens with a higher RDX ratio also have a lower expansion ratio and porosity.

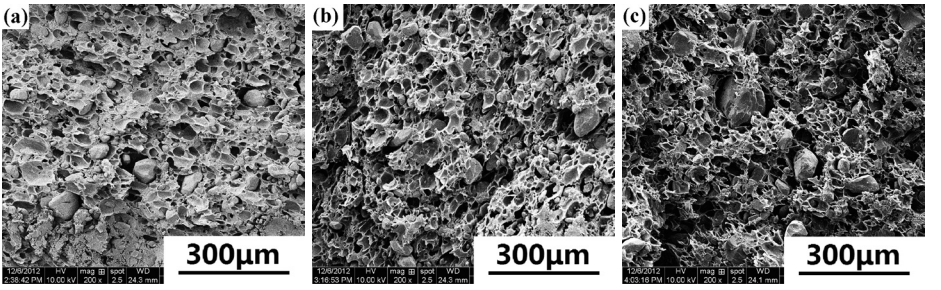

Figure 7. SEM micrographs of specimens with different RDX ratios (temperature = 50 °C, pressure = 20 MPa, time = 10 s): (a) 50%; (b) 60%; (c) 70%.

Table 4. Structural parameters of specimens with different RDX ratios

RDX ratio [%]	ρ_s [g/cm^3]	ρ_f [g/cm^3]	φ	V [%]	N_0 [cells/cm^3]
50	1.36	0.70	1.94	48.5	3.7×10^7
60	1.50	0.83	1.81	44.8	3.9×10^7
70	1.61	0.94	1.74	42.5	4.2×10^7

3.2.5 Skin-core structure

The skin-core structure of a foamed specimen is shown in Figure 8. This clearly shows that although there are many microcells inside the material, none are observed on the surface. It appears that gas in the surface region readily escapes during the process of sudden pressure quench and no nucleation occurs.

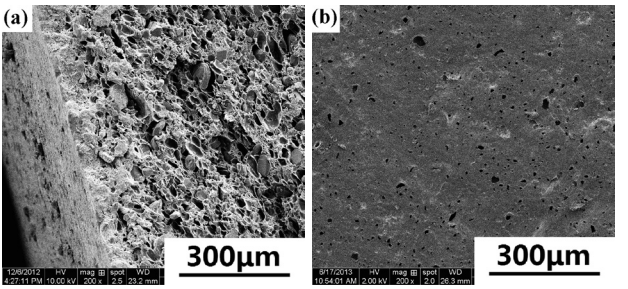

Figure 8. Skin-core structure (pressure = 15 MPa, temperature = 60 °C, time = 10 s): (a) vertical section; (b) surface.

3.3 Mechanical sensitivities

The friction and impact sensitivities of samples with various RDX contents were tested and the results are listed in Table 5. The mean explosion probability of friction sensitivity is 0 for each sample, revealing good friction sensitivity. The characteristic drop height ($\overline{H}_{50}$) decreased with increased RDX ratio.

Table 5. Mechanical sensitivities of different samples

Sample	Friction sensitivity	Impact sensitivity	
	$\overline{P}$ [%]	$\overline{H}_{50}$ [cm]	$S_{dev.}$
50% RDX	0	30.34	0.2440
60% RDX	0	29.85	0.0833
70% RDX	0	27.99	0.058

3.4 Burning characteristics

The typical *p-t* curves of a single-base propellant and microcellular combustible material are shown in Figure 9. Compared with a traditional propellant, foamed samples exhibit vastly differing combustion characters, particularly in the ignition stage. Single-base propellants are ignited before the ignition powder has burned out. However, the *p-t* history of a foamed specimen is composed of the ignition and combustion of the ignition powder, as well as the ignition and combustion of the specimen. In addition, the pressure increased slowly with time in the initial combustion stage. Table 6 presents the burning time (t_m) and maximum pressure (p_m) data from the closed vessel tests. As the data indicate, the burning time of foamed specimens was markedly decreased owing to the decreased density or an increased RDX content.

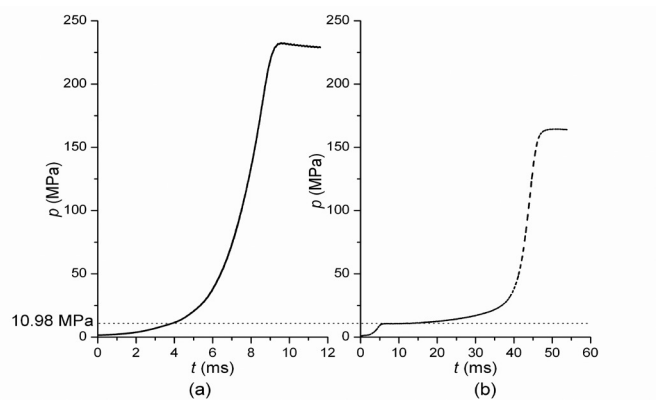

Figure 9. *p-t* curves of: (a) a single-base propellant, and (b) a foamed specimen with 60% RDX at 20 MPa and 40 °C.

Table 6. Values of t_m and p_m from the *p-t* curves of different samples

Samples	t_m, [ms]	p_m, [MPa]
50% RDX unfoamed	540.38	121.64
60% RDX unfoamed	190.78	163.64
70% RDX unfoamed	70.53	194.37
50% RDX, 40 °C, 20 MPa	154.77	133.97
60% RDX, 40 °C, 20 MPa	56.03	164.61
60% RDX, 50 °C, 20 MPa	32.97	164.44
60% RDX, 60 °C, 20 MPa	36.84	164.41
70% RDX, 40 °C, 10 MPa	27.19	202.57
70% RDX, 40 °C, 20 MPa	29.51	201.85

Note: burning time (t_m) was measured in ms from 10.98 MPa to p_m.

4 Conclusions

(1) Specimens with different porous structure can be produced by adjusting the foaming conditions.
(2) Foamed specimens show good friction vulnerability.
(3) The materials are hard to ignite in a closed bomb, and show good heat resistance from another point of view.
(4) Relationships between the foaming parameters, the burning characteristics and the ballistic performance need to be investigated in subsequent work.

Acknowledgments
Funding by the Priority Academic Program Development of Jiangsu Higher Education Institutions is gratefully acknowledged.

5 References

[1] Messmer A., Pfatteicher A., Schmid K., Kuglstatter W., Foamed Propellants with Energetic Binders, *31st Int. Annu. Conf. ICT*, Karlsruhe, Germany, **2000**, 111/1-13.
[2] Shedge M., Patel C.H., Tadkod S.K., Murthy G.D., Polyvinyl Acetate Resin as a Binder Effecting Mechanical and Combustion Properties of Combustible Cartridge Case Formulations, *Def. Sci. J.*, **2008**, *58*(3), 390-397.
[3] DeLuca P.L., Williams J.C., Fibrillated Polyacrylic Fiber in Combustible Cartridge Cases, *Ind. Eng. Chem. Prod. Res. Dev.*, **1984**, *23*(3), 438-441.
[4] Zimmerman F., Development of 7.62-mm and 38-mm Combustible Cartridge Case Ammunition, *J. Spacecr. Rockets*, **1969**, *6*, 312-314.
[5] Kurulkar G.R., Syal R.K., Singh H., Combustible Cartridge Case Formulation and Evaluation, *J. Energ. Mater.*, **1996**, *14*(2), 127-149.
[6] Böhnlein-Mauß J., Kröber H., Technology of Foamed Propellants, *Propellants Explos. Pyrotech.*, **2009**, *34*(3), 239-244.
[7] Böhnlein-Mauß, J., Eberhardt A., Fischer T.S., Foamed Propellants, *Propellants Explos. Pyrotech.*, **2002**, *27*(3), 156-160.
[8] Fischer T.S., Messmer A., Burning Characteristics of Foamed Polymer Bonded Propellants, *19th Int. Symposium of Ballistics*, Interlaken, Switzerland, **2002**, 139-139.
[9] Li Y., Yang W., Ying S., Preparation and Characteristics of Foamed NC-based Propellants, **2014**, *Propellants Explos. Pyrotech.*, in press.
[10] Ying S.J., Xu F.M., Research on Supercritical Fluid Foaming Technology for Preparation of Microcellular Foamed Propellants, *Acta Armamentarii (Binggong Xuebao)*, **2013**, *34*(8), 1028-1036.
[11] Chen X.R., Ying S.J., Xiao Z.G., Research on Preparation of Microfoam Oblate

Spherical Propellants by Supercritical CO_2, *Acta Armamentarii (Binggong Xuebao)*, **2012**, *5*, 534-539.

[12] Zhu B., Zha W., Yang J., Zhang C., Lee L.J, Layered-silicate Based Polystyrene Nanocomposite Microcellular Foam Using Supercritical Carbon Dioxide as Blowing Agent, *Polymer*, **2010**, *51*(10), 2177-2184.

[13] Reverchon E., Cardea S., Production of Controlled Polymeric Foams by Supercritical CO_2, *J. Supercrit. Fluids*, **2007**, *40*(1), 144-152.

[14] Xu Q., Xianwen Ren X., Chang Y., Wang J., Yu L., Dean K., Generation of Microcellular Biodegradable Polycaprolactone Foams in Supercritical Carbon Dioxide, *J. Appl. Polym. Sci.*, **2004**, *94*(2), 593-597.

[15] Ruiz J.A.R., Viot P., Dumon M., Microcellular Foaming of Polymethylmethacrylate in a Batch Supercritical CO_2 Process: Effect of Microstructure on Compression Behavior, *J. Appl. Polym. Sci.*, **2010**, *118*(1), 320-331.

[16] Yang W., Li Y., Ying S., Fabrication Thermoanalysis and Performance Evaluation Studies on RDX-based Microcellular Combustible Objects, **2014**, *Propellants Explos. Pyrotech.*, in press.

[17] Colton J.S., Suh N.P., Nucleation of Microcellular Foam: Theory and Practice, *Polym. Eng. Sci.*, **1987**, *27*(7), 500-503.

[18] Colton J.S., Suh N.P., The Nucleation of Microcellular Thermoplastic Foam: Process Model and Experimental Results, *Mater. Manuf. Processes*, **1986**, *1*(3-4), 341-364.

[19] Colton J.S., Suh N.P., The Nucleation of Microcellular Thermoplastic Foam with Additives: Part I: Theoretical Considerations, *Polym. Eng. Sci.*, **1987**, *27*(7), 485-492.

[20] Goel S.K., Beckman E.J., Generation of Microcellular Polymeric Foams Using Supercritical Carbon Dioxide. II: Cell Growth and Skin Formation, *Polym. Eng. Sci.*, **1994**, *34*(14), 1148-1156.